

RADIATION HYDRODYNAMICAL EVOLUTION OF PRIMORDIAL H II REGIONS

DANIEL WHALEN

Department of Physics, University of Illinois, Urbana-Champaign, Urbana, IL 61801
dwhalen@cosmos.ucsd.edu

TOM ABEL

Pennsylvania State University, University Park, PA 16802

AND

MICHAEL L. NORMAN

University of California, San Diego, La Jolla, CA 92093

Draft version February 5, 2008

ABSTRACT

We simulate the ionization environment of $z \sim 20$ luminous objects formed within the framework of the current CDM cosmology and compute their UV escape fraction. These objects are likely single very massive stars that are copious UV emitters. We present analytical estimates as well as one-dimensional radiation hydrodynamical calculations of the evolution of these first HII regions in the universe. The initially D-type ionization front evolves to become R-type within $\lesssim 10^5$ yrs at a distance ~ 1 pc. This ionization front then completely overruns the halo, accelerating an expanding shell of gas outward to velocities in excess of 30 km s^{-1} , about ten times the escape velocity of the confining dark matter halo. We find that the evolution of the HII region depends only weakly on the assumed stellar ionizing luminosities. Consequently, most of the gas surrounding the first stars will leave the dark halo whether or not the stars produce supernovae. If they form the first massive seed black holes these are unlikely to accrete within a Hubble time after they formed until they are incorporated into larger dark matter halos that contain more gas. Because these I-fronts exit the halo on timescales much shorter than the stars' main sequence lifetimes their host halos have UV escape fractions of $\gtrsim 0.95$, fixing an important parameter for theoretical studies of cosmological hydrogen reionization.

Subject headings: cosmology: theory—early universe—HII regions: simulation

1. INTRODUCTION

In light of recent WMAP results on reionization (Kogut *et al.* 2003) there has been renewed interest in early reionization scenarios (Haiman & Holder 2003; Cen 2003; Somerville & Livio 2003; Barkana & Loeb 2003; Sokasian, Abel, Hernquist, & Springel 2003; Ciardi, Ferrara, & White 2003; Ciardi, Ferrara, Marri, & Raimondo 2001). The models rely heavily on UV production estimates for the assumed stellar populations and the escape rates depending on the global structure of the luminous proto-galaxies. The latter is modeled by an escape fraction, f_{esc} , which is defined as the fraction of ionizing photons produced by stars within a luminous object that exit the object.

1.1. Previous UV Escape Fraction Estimates

Initial upper limits of only 0.02–0.15 placed upon escape fractions for local starburst galaxies (Leitherer *et al.* 1995) raised concerns about the role early galaxies could have had in reionization but these estimates were later revised upward by a factor of four (Hurwitz, Jelinsky, & Dixon 1997). Lyman break galaxies may have escape fractions greater than 0.2 (Steidel *et al.* 2001). Theoretical investigations usually derive very low escape fractions for even small high redshift galaxies in part because of the assumed scaling of the typical interstellar densities with $(1+z)^3$ (Wood & Loeb 2000; Ricotti & Shull 2000). Wood & Loeb (2000) in particular do not consider radiation-driven hydrodynamic motion in their static models that could open channels out the galaxy from which UV flux might escape. A notable exception is the study by Fujita *et al.* (2003)

which does model galactic outflows with multidimensional hydrodynamical simulations and finds an appreciably larger escape fraction of $\gtrsim 20\%$.

Unfortunately, there is a clear limit to how far present upper bounds on f_{esc} can predict the escape of UV photons from Pop III stars because the ionization environment of primordial stars residing in minihalos at $z \sim 20$ is very different from that observed in $z \lesssim 0.1$ galaxies. Zero-metallicity Pop III stars are not currently thought to have line-driven stellar winds (Baraffe, Heger, & Woosley 2001; Kudritzki 2000; Vink, de Koter, & Lamers 2001) or exhibit instabilities that can drive significant mass loss on timescales smaller than the main sequence lifetimes of these stars. Consequently, the wind bubbles blown by OB associations in galactic settings which can act to trap UV outflow from these stars (Dove, Shull, & Ferrara 2000) are probably absent around Pop III stars so we do not consider them in our study. Likewise, the primordial halos surrounding the first generation of stars were free of dust that impedes escape of UV photons in modern galaxies. UV escape fractions and their evolution in current models of early reionization have therefore remained highly uncertain and been treated as a free parameter.

Of similar importance in these models is the efficiency of UV photon production per baryon in stars. Interestingly, different stellar population synthesis models disagree on UV production efficiency, regardless of IMF (see e.g. Schaerer (2002) or Wise & Abel (2002) for a discussion). Fortunately, high-resolution CDM hydrodynamical simulations now offer robust predictions of the masses and evolution of the first luminous objects that can guide studies of early reionization.

1.2. Geometry and Masses of Simulated First Luminous Objects

Several different techniques have been applied to numerical simulations of the first stars. The initial studies using nested grid Eulerian schemes (Abel 1995; Abel *et al.* 1998) revealed that the first cosmological objects condense cool $1000 M_{\odot}$ clouds in their centers. At that time we argued that insufficient spatial resolution and the exclusion of three body formation of molecular hydrogen (Palla *et al.* 1983; Silk 1983) left the fate of these large clouds uncertain. Similarly medium-resolution smooth particle hydrodynamics simulations (Bromm *et al.* 1999) that followed the idealized collapse of uniformly rotating spheres of masses of $2 \times 10^6 M_{\odot}$ also found cold clouds of masses $\sim 10^3 M_{\odot}$ to form. These rotating models first create rotationally-supported disks that eventually fragment. In contrast, simulations that account for the full hierarchy of structure in CDM models from realistic cosmological conditions produce no disks (Abel 1995; Abel *et al.* 1998; Fuller & Couchman 2000; Abel *et al.* 2000; Machacek *et al.* 2001; Yoshida, Abel, Hernquist, & Sugiyama 2003), independent of whether smooth particle hydrodynamical or Eulerian adaptive mesh refinement (AMR) techniques are employed. Instead, these studies typically find the first protostellar objects to be roughly spherical on scales from ~ 0.1 pc out to the virial radii (~ 100 pc), with masses of approximately $100 M_{\odot}$ accreting within dark matter halos on the order of $10^6 M_{\odot}$ and forming by redshifts of 20 - 30. This absence of global disks in the first galaxies and hence around the first luminous objects is crucial to understanding their UV escape fraction and the impact of the first supernova explosions. For a first study of the formation and evolution of the first HII regions, however, it is reasonable to employ only one dimensional radiation-hydrodynamical models.

The highest resolution simulations to date with elements as small as $\sim 100 R_{\odot}$ and $\sim 1/4 M_{\odot}$ (Abel *et al.* 2002), which also include three-body molecular hydrogen formation, suggest that the primordial molecular cloud analogs do not fragment. They instead form a single very massive star from the inside out. The detailed processes limiting the accretion onto these first protostars are not fully understood but Abel *et al.* (2002) suggested a plausible mass range for the first stars to be between 30 and $300 M_{\odot}$.

Subsequent studies of Omukai & Palla (2003) assert that the first stars might be as large as $600 M_{\odot}$, at which point accretion times from Abel *et al.* (2002) become equal to the lifetime of a primordial massive star. However, as discussed in detail by Heger & Woosley (2002) such massive stars would most likely bypass SN explosion to form black holes directly without releasing the heavy elements necessary for the formation of the next generation of lower-mass metal-enriched stars. Omukai & Palla further argued that these stars would never achieve photospheric temperatures in excess of 6000 K to contribute UV radiation to the early reionization of the universe.

The models of Omukai and Palla do not include full hydrodynamics and perhaps more importantly only consider grey radiative transport using mean opacities. Grey transport may fail to capture UV photons in the Lyman Werner bands of H_2 which even in small numbers will destroy H_2 in the accreting envelope that cannot be reformed because of the absence of dust and free electrons. This method may therefore fail to properly cut off the H_2 cooling that permits accretion to continue, leading to overestimates of protostellar mass. Considering the three-dimensional nature of the accretion, it also seems unlikely

that the material would accumulate at the exact rate required to keep the star from reaching the 100,000 K ZAMS temperatures predicted by theory (Schaerer 2002). However, see Omukai & Palla (2003) and Omukai & Inutsuka (2002) for a markedly different view. We feel that only fully three-dimensional radiation hydrodynamical simulations that follow radiative transfer without resorting to grey opacities will be able to shed light on the exact physics that presumably halt the accretion of the first protostars. Therefore, given that ab initio numerical simulations yield the detailed structure of the first star-forming clouds and good estimates for the range of expected luminosities of the first stars are available, it is timely to discuss the properties of the associated first HII regions. In this paper we demonstrate that the escape fraction from most microgalaxies holding very massive primordial stars is of order unity. We make this point with one dimensional radiation hydrodynamical simulations along with purely analytical arguments. In light of the possible overestimates of final primordial star masses in some current work we only consider the 120 – 500 M_{\odot} mass range of interest also to future SN metal mixing studies.

2. REACTIVE FLOW AND RADIATIVE TRANSFER IN ZEUS-MP

Collisional and ionization processes can ionize and recombine primordial H and He into H^+ , He^+ , He^{2+} , H^- , H_2^+ , H_2 , and e^- , which we added to ZEUS-MP by insertion of a 9-species reaction network and nine additional advection equations (Abel *et al.* 1997; Anninos *et al.* 1997). For simplicity, the calculations we present here assume the primordial gas is hydrogen only, which can be in neutral or ionic form but not molecular. We discuss the omission of helium later and show that it has a minimal effect on our principal conclusions. The rate equation for change of neutral hydrogen abundance (excluding the advection term) reduces to:

$$\frac{dn_H}{dt} = k_{rec}n_{H^+}n_e - k_{ph}n_H - k_{coll}n_Hn_e \quad (1)$$

We further modified ZEUS-MP to follow the radiative transfer of a single point source of UV radiation at the center of a spherical-coordinate geometry. Photoionizations in any given cell are due to direct photons from the central source entering the cell's lower face as well as to diffuse photons entering through all its faces. Recombinations within a zone occur to both the ground state and to all the excited states. The on-the-spot approximation (Osterbrock 1989) allows us to equate the diffuse ionizations in a cell to its recombinations to the ground state, relieving us of the costly radiative transfer from many lines of sight needed to compute the diffuse radiation in the cell. The diffuse ionization and ground-state recombination terms cancel each other in the network above so only a single integration of the transfer equation along a radial ray from the coordinate center is necessary to compute k_{ph} in a zone.

Recognizing that light-crossing times over most of the problem domain are short in comparison to material evolution timescales enables us to discard the time derivative in the equation of transfer that would otherwise restrict the code to unnecessarily short timesteps. Rapid ionizations very close to the central star will violate this approximation and lead to superluminal I-front velocities, which we prevent by computing fluxes only at distances smaller than $ct_{problem}$ from the star (see Abel, Norman, & Madau (1999) for discussion). In practice, the static approximation to the equation of transfer usually becomes valid before the I-front approaches the Strömgen radius

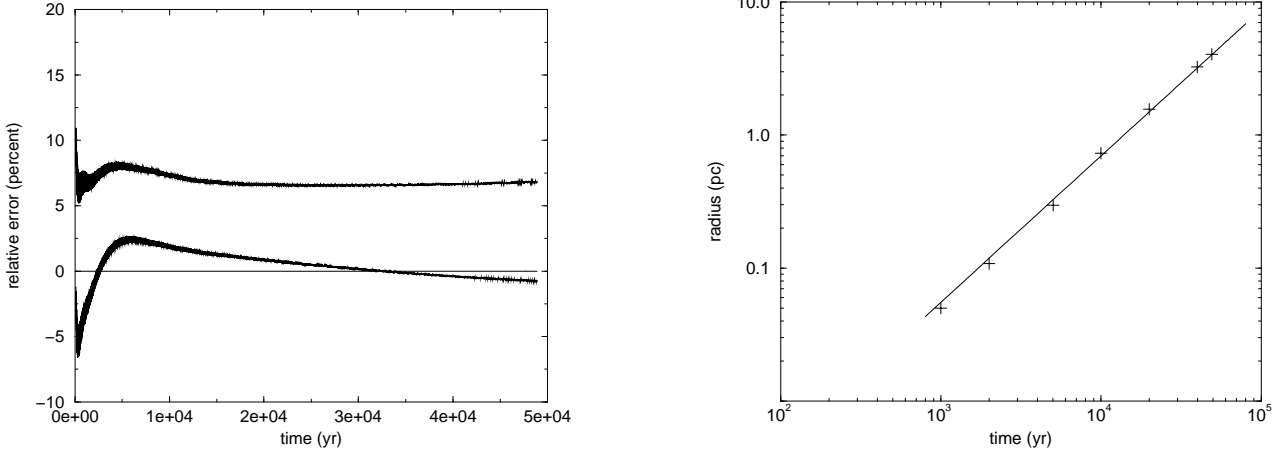


FIG. 1.— ZEUS-MP propagation of I-fronts down r^{-1} (left) and r^{-3} (right) density gradients. The left panel displays the percent error in position between the ZEUS-MP leading shock and I-front calculations and the Franco *et al.* (1990) prediction. The upper and lower curves are the shock and front, respectively. The right panel compares ZEUS-MP core shock positions with theory (the I-front having already exited the halo).

and the code computes Strömgren radii and formation times in excellent agreement with theory.

Hence, we solve the static equation of radiative transfer in flux form

$$\nabla \cdot \mathbf{F} = -\chi \mathbf{F}_r, \quad \chi = \frac{1}{n\sigma}$$

to produce the central flux piercing the bottom of each cell

$$F_i = \left(\frac{r_{i-1}}{r_i} \right)^2 F_{i-1} e^{-\chi(r_i - r_{i-1})} \quad (2)$$

which yields the photoionization rate coefficient k_{ph} with units [1/s] for the i^{th} radial zone:

$$k_{ph} = \frac{F_i (1 - e^{-\chi(r_{i+1} - r_i)}) A_{inner}}{h\nu n_H V_{cell}} \quad (3)$$

where V_{cell} and A_{inner} are the volume and area of the lower face of the cell. This numerical scheme ensures conservation of photons in all problem zones, a highly-desirable property that ensures I-fronts propagate at speeds that are independent of problem resolution. We consider only monochromatic radiative transfer, wherein a fixed amount of heat ϵ_Γ is deposited by the radiation per photoionization. Though not necessary for 1-D studies, this restriction greatly reduces computational cost and will allow full three-dimensional simulations (Whalen *et al.* in preparation).

Photoionization, collisional ionization and recombination processes can occur over highly disparate timescales that are all in general much shorter than the hydrodynamic response of the gas. We finite difference the reaction network in a semi-implicit scheme which employs densities at the advanced time but rate coefficients evaluated at the current time. This algorithm bypasses costly matrix iteration that would become prohibitive in 3-D while retaining sufficient accuracy to follow I-front propagation. The code subcycles the reaction network and isochoric energy equation by a tenth of the photoionization timestep

$$t_{chem} = \frac{n_e}{\dot{n}_e} \quad (4)$$

until it has covered a tenth of the heating/cooling timestep

$$t_{heat/cool} = \frac{e_{gas}}{\dot{e}_{heat/cool}} \quad (5)$$

at which point it updates the hydro equations.

The absence of metals in the first-generation stars and their primordial envelopes permits the use of simple cooling rates in the isochoric energy equation. Only photoionization, recombination, electron collisional ionization and excitation occur in the atomic hydrogen we consider in our calculations, yielding the energy equation:

$$\dot{e}_{gas} = k_{ph} \epsilon_\Gamma n_H - \Lambda_{rec} n_H n_e - \Lambda_{coll ioniz} n_H n_e - \Lambda_{coll exc} n_H n_e \quad (6)$$

where k_{ph} is the photoionization rate described above, ϵ_Γ is the fixed energy per ionization deposited into the gas (set to 2.4 eV for reasons explained in Section 5), and Λ_{rec} , $\Lambda_{coll ioniz}$, and $\Lambda_{coll exc}$ are the recombinational and collisional cooling rates taken from Anninos *et al.* (1997)). These four processes act in concert with hydrodynamics (such as adiabatic expansion or shock heating) to set the temperature of the gas everywhere in the simulations.

3. CODE TESTS

We adopted the benchmarks that Franco *et al.* (Franco *et al.* 1990; Tenorio-Tagle *et al.* 1986) employed in their theoretical studies of I-front propagation, in which a source of ionizing photons was centered in a radial density profile with a flat core and an $r^{-\omega}$ dropoff:

$$n_H(r) = \begin{cases} n_c & \text{if } r \leq r_c \\ n_c(r/r_c)^{-\omega} & \text{if } r \geq r_c \end{cases}$$

We applied the same initial density profiles, central source strength, and cooling physics in our tests as did Franco, *et al.* Their studies of I-front propagation down these radial density gradients indicate there is a critical exponent $\omega = 1.5$ below which the front executes the classic approach to a Strömgren sphere, reverts from R-type to D-type, and subsequently

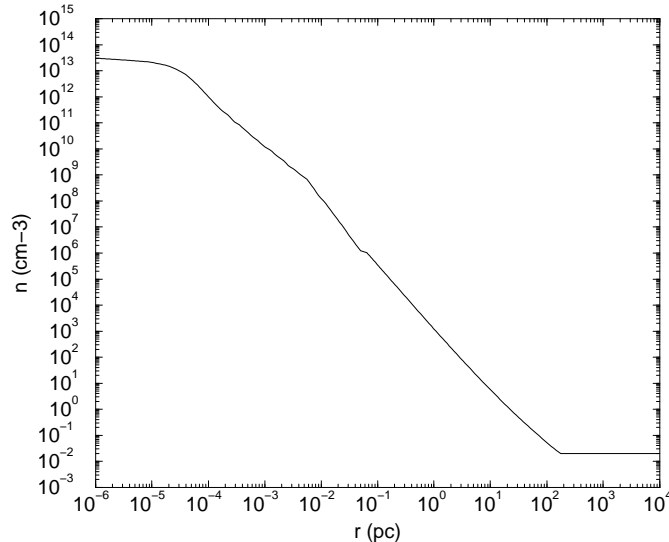


FIG. 2.— Primordial cloud number density from Abel *et al.* (2002).

drives a dense shocked shell before it thereafter down the density gradient (Franco *et al.* 1990). The front remains D-type throughout its evolution and accumulates mass in its shell for as long as it expands. Fig 1 compares ZEUS-MP’s propagation of a D-type I-front down an r^{-1} density gradient to the predicted analytical result. The code results agree with theory to within 7% at early times and 3% at later times. We expect slightly greater disagreement at early times because no current theory addresses the hydrodynamic details of the R- to D-transition but becomes increasingly accurate as the I-front evolves. The shock front can be seen to precede the I-front with the analytical result (which assumes the shock and front positions essentially coincide) falling between them.

Ionization fronts descending density gradients steeper than the critical $\omega = 1.5$ rapidly revert from D-type back to R-type (in some cases never having switched from R-type in the first place) and quickly overrun the cloud. Now completely ionized and at much higher pressures, the entire cloud inflates outward at the sound speed of the ionized material, typically on the order of 10 km s^{-1} . In this scenario strong core density gradients in the now mostly-isothermal cloud become strong pressure gradients which drive a shock that pistons the already-moving cloud material outward in a champagne flow. The shocked core expands at nearly constant velocities down $1.5 < \omega < 3$ gradients but strongly accelerates out through $\omega > 3$ gradients. Runs conducted with ZEUS-MP for $1.5 < \omega < 5$ demonstrate this behavior. Fig 1 compares ZEUS-MP’s expansion of the ionized core to the core expansion rates of the Franco *et al.* (1990) theory, demonstrating agreement to within 10% at early times and 2% at later times.

4. SIMULATION SET UP

We show in Fig 2 the fit we computed to the spherically-averaged gas number density surrounding the primordial protostar of the very high dynamical range AMR calculation performed by Abel *et al.* (2002). In that calculation the protostellar core accreted within a $7 \times 10^5 M_{\odot}$ dark matter halo by a redshift of 18.2. At $r \sim 175 \text{ pc}$ we smoothly joined this fit to a constant baryon number density of 0.02 cm^{-3} , which is roughly 10 times the cosmic mean at this redshift, to approximate the higher circum-halo density found in Abel *et al.* (2002). In Ta-

ble 2 we list final I-front radii assuming a circum-halo density equal to the cosmic mean. The spherical averaging of the baryonic density removes clumping and other features whose effects will be studied when we extend these simulations to 3-D in a forthcoming paper.

The density was assigned a uniform temperature of 300 K (typical of the virialized baryonic matter cooled by molecular hydrogen in the Abel *et al.* (2002) simulations) and made static by applying the gravitational potential necessary to hold it in hydrostatic equilibrium (this potential would be that exerted by the dark matter halo were it explicitly present in our simulation). We evolved this model without a central ionizing source to make certain the gas is in sufficiently stable equilibrium and found peculiar velocities to be less than 0.1 km s^{-1} after the three million years typical for lifetimes of very massive primordial stars. The gravitational potential was held constant throughout the evolution of the problem because the exit of the gas from the halo should have minimal impact on the more massive equilibrium dark matter halo left behind. For the results presented below we used 142 logarithmically-spaced radial zones. We placed a series of constant ionizing luminosities shown in Table 1 corresponding to a range of stellar masses and main-sequence lifetimes (Schaerer 2002) at the center of the distribution (the $120 M_{\odot}$ star was what emerged from the Abel *et al.* (2002) calculations).

Table 1: Ionizing Photon Rates and Main Sequence Lifetimes

M_{\odot}	main sequence lifetime (yrs)	\dot{n}_{ph}
500	1.899e06	6.802e50
400	1.974e06	5.247e50
300	2.047e06	3.754e50
200	2.204e06	2.624e50
120	2.521e06	1.391e50

These constant hydrogen ionization luminosities were obtained by averaging the stars’ time-varying outputs over their main sequence lifetimes, assuming no mass loss (Schaerer 2002). Time-dependent luminosities are easily incorporated into the code and will be included in later 3D studies where their effects

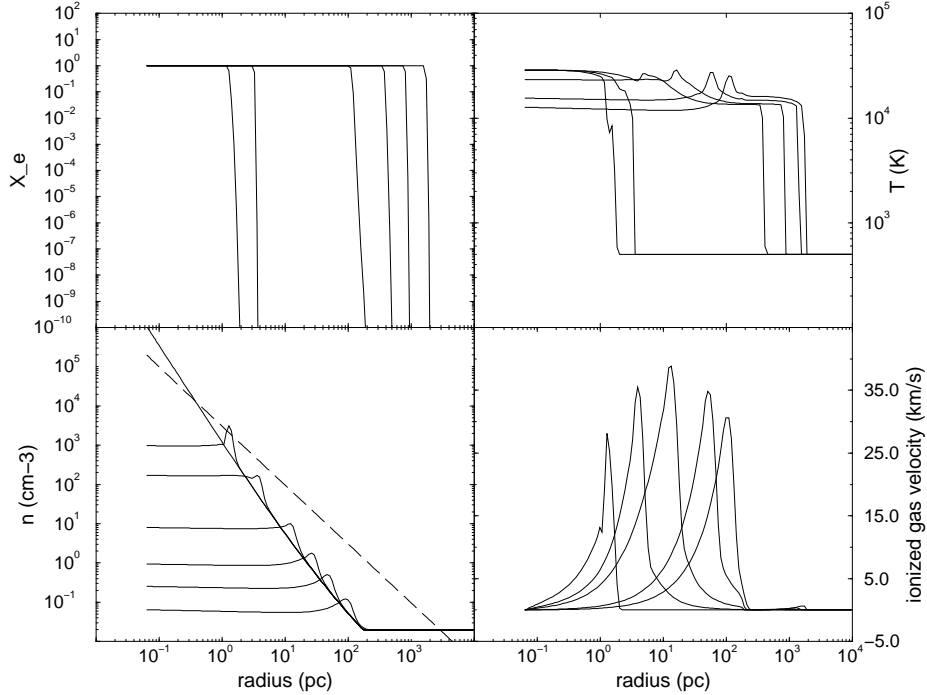


FIG. 3.— Expansion of an HII region from a $200 M_{\odot}$ star. The ionization fraction profiles are shown for $t = 63$ kyr, 82 kyr, 95 kyr, 126.9 kyr, 317 kyr, and 2.2 Myr. The temperature distributions are output for $t = 63$ kyr, 82 kyr, 126.9 kyr, 317 kyr, 1.11 Myr, and 2.2 Myr, and the densities are shown for $t = 0$ yr, 63 kyr, 126.9 kyr, 317 kyr, 634 kyr, 1.11 Myr, and 2.2 Myr. The velocity profiles shown are for $t = 63$ kyr, 126.9 kyr, 317 kyr, 1.11 Myr, and 2.2 Myr. The dashed line in the density panel is the Strömgren density (the density required to form a Strömgren sphere and therefore initially bind the I-front) at a given radius.

may be more pronounced.

5. RESULTS AND DISCUSSION

5.1. A Standard Case

In non-rotating stellar evolution models stars above $50 M_{\odot}$ and below $140 M_{\odot}$ as well as above $260 M_{\odot}$ likely avoid supernova explosions and collapse directly into black holes (Heger & Woosley 2002). We examined first the HII region formed by a $200 M_{\odot}$ star to understand the environment into which a primordial pair-instability supernova would detonate to produce metal enrichment. Fig 3 displays the ionization, temperature, density, and velocity profiles of the HII region expanding outward from this star for the output times listed. Initially the D-type ionization front is trapped as expected (Franco *et al.* 1990) and a shock forms ahead of the front. The first two temperature profiles capture the I-front just as it reverts from D-type back to R-type. At 82 kyr the 25000 K front has just overtaken the 7000 K shock that had been leading at 63 kyr. The I-front then abruptly descends the density gradient from 3 pc to 100 pc over the next 15 kyr as seen in the third ionization profile, setting all of the ionized gas into outward motion. The strong density jump just before the front at 63 kyr is gone at 126 kyr as the front advances well ahead of the shock leaving essentially undisturbed (though much hotter) gas in its wake.

One can apply a simple analytical argument to obtain a rough estimate of where the front reverts to R-type by computing the Strömgren density at a given radius assuming no hydrodynamic motion:

$$n_S = \left(\frac{3F_*}{4\pi\alpha_B} \right)^{\frac{1}{3}} r^{-\frac{3}{2}}, \quad (7)$$

where F_* is the number of ionizing photons per second from the star. This is the density required to stall the early front to a Strömgren radius before hydrodynamic motions free it to advance forward. n_S appears as the dashed line on the density panel in Fig 3. The initial density profile can temporarily trap the I-front wherever it is greater than n_S but not when it dips below it, so one would expect the I-front to revert to R-type beyond that radius. In reality this transition is delayed when the front encounters and must also ionize the overdense shock. The delay is evident when comparing the ionization and density profiles because the $t = 0$ density drops below n_S at 0.4 pc but the front does not overtake the shock until 3 pc.

Once again R-type, the front rapidly inflates outward on timescales much shorter than the hydrodynamic response of the gas. The gas motion that follows this abrupt ionization becomes apparent in the later temperature, density and velocity profiles in Fig 3. Just as in the Franco benchmarks, strong density gradients in the now ionized and nearly isothermal gas (as seen in the temperature plots) become strong pressure gradients beyond the edge of the density's flat central core which drive a shock out into the ionized gas. The shock weakly accelerates but achieves velocities in excess of 35 km s^{-1} in comparison to the 12 - 15 km s^{-1} sound speed of the 15000 K gas and the 2 - 3 km s^{-1} escape velocity from the halo. The small velocity bumps beyond 1 kpc in the final two velocity profiles are due to the outer edge of the front slowing down to a new Strömgren radius as it traverses the constant interhalo mean density. The velocities growing there will steepen into a shock behind the front that would eventually overtake it if the central star continued to shine.

The temperature peaks at later times that coincide with the

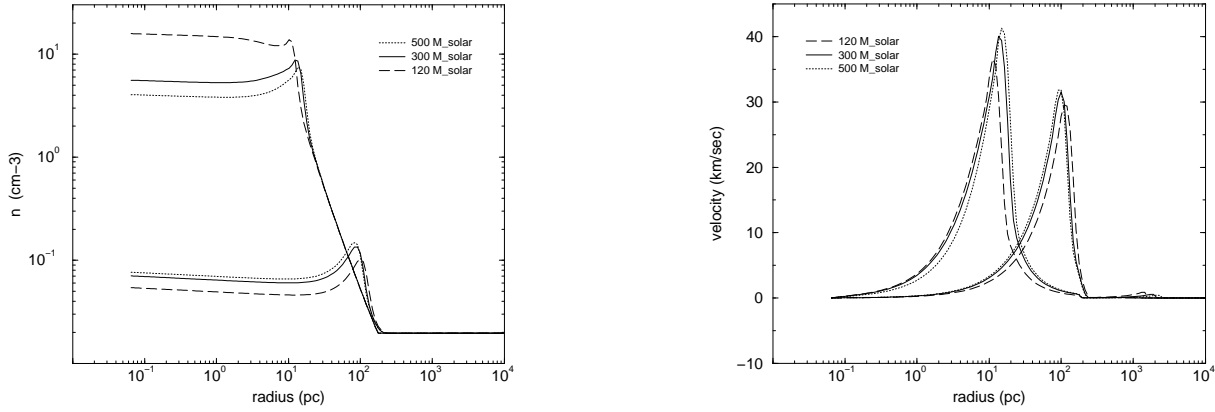


FIG. 4.— Left panel: HII region density profiles for $120 M_{\odot}$, $300 M_{\odot}$, and $500 M_{\odot}$ central stars. The densities shown are for 317.1 kyr and then again at the main sequence cutoff time of each star: 2.5, 2.0 and 1.9 Myr, respectively. Right panel: Velocity profiles for $120 M_{\odot}$, $300 M_{\odot}$, and $500 M_{\odot}$ central star HII regions. The velocities shown are for 317.1 kyr and then again at the main sequence cutoff time of each star: 2.5, 2.0 and 1.9 Myr.

velocity peaks are from shock heating. The postshock gas temperature gradually decreases with time from adiabatic expansion, recombinational cooling, and electron-ionization, and -excitation cooling processes in the primordial hydrogen. The preshock gas is hotter than the postshock gas since it has not had as much time to cool and will be heated by the shock's passage.

The time-sequenced density profiles clearly show the flow of photoionized gas out of the halo, with the flat postshock densities gradually draining away to twice the interhalo mean. The shock and density peaks reach the 100 pc virial radius of the halo by the star's main sequence lifetime. Nearly half the gas originally interior to 100 pc has flowed out by this time as seen in Fig 5, which plots the total gas mass enclosed within a given radius for the three output times listed. The uppermost curve is the original undisturbed halo gas. The difference between this curve and the later ones at any radius is a measure of how much material has been driven from that radius. At 2.2 Myr $6000 M_{\odot}$ of the initial $15000 M_{\odot}$ present has crossed over 100 pc. The ionized flow is efficient at expelling gas from the interior of the halo, leaving its innermost 50 pc at only twice the intergalactic mean density. Because the shock sweeps the bulk of the expelled material outward at velocities well in excess of the $2 - 3 \text{ km s}^{-1}$ escape velocity from the halo, its return to the halo on merger timescales is unlikely.

5.2. Varying the Ionizing Luminosity

We computed four additional cases having the same initial density profile but with the different luminosities in Table 1. The HII regions in each case follow the same evolutionary stages as in the $200 M_{\odot}$ run. HII densities and velocities for $120 M_{\odot}$, $300 M_{\odot}$, and $500 M_{\odot}$ central stars are shown in Fig 4, first at 0.6 Myr and then at the main sequence cutoff times 2.5, 2.0 and 1.9 Myr of each, respectively.

It is immediately apparent from both plots that the ionized flow's characteristics are largely independent of central photon rates. The peak shock speeds differ by at most 5 km s^{-1} even though the luminosities vary by a factor of 5. The relatively minor variation in shock velocities leads to the small spread in shock positions seen at the two times in the density plot. The R-type front leaves the halo ionized on timescales short in comparison to the subsequent flow times so the initial ionized density left in its wake is not very different from the original profile, the same used in all the luminosities we considered. Because

it is the density and pressure gradients left by the front (and not the front itself or the luminosity that drove it) that govern the hydrodynamics of the resultant photoevaporation, it is reasonable to expect different luminosities to deliver the same ionized flows. I-front dynamics in the core are responsible for the spread in shock speeds. Fronts driven by greater luminosities leave slightly steeper ionized densities behind at the core edge. The accompanying steeper pressure falloff accelerates the gas to the slightly greater speeds seen in the higher luminosity runs.

At 0.6 Myr the postshock densities are lowest for the brightest star as one might expect because its somewhat faster core shock pushes matter from the halo more quickly. In contrast, the dimmest star leaves the smallest densities in the halo at its main sequence lifetime, but only because the same photoevaporative outflow present in all three cases has been acting for the longest time. Our simulations show that the ionized outflow from the more massive stars persists well after their shutoff. In Fig 6 we plot the density profiles left by the three stars at 2.5 Myr, shutting down the central source after the star's MSL but permitting recombinational, electron collisional, and hydrodynamical processes to continue. If allowed to act in the absence of a supernova, post-MSL outflow from the more massive stars would evacuate the halo more completely than the longer-lived dimmer stars, as also evident in Fig 5.

We reran these calculations with the same halo but with an intercluster baryon density of 0.00135 corresponding to a redshift of 18.2 for a standard cosmology with $\Omega_B h^2 = 0.0224$ consistent with the recent WMAP results (Spergel et al. 2003) and the primordial deuterium abundance measurements by Burles & Tytler (1998) to compute the final volumes ionized by the five luminosities. The final I-front position for each is listed in Table 2. As expected, the brightest stars ionize the greatest volumes.

Table 2: Final I-front Radii

M_{\odot}	final I-front position (pc)
500	5363
400	5080
300	4558
200	3874
120	3120

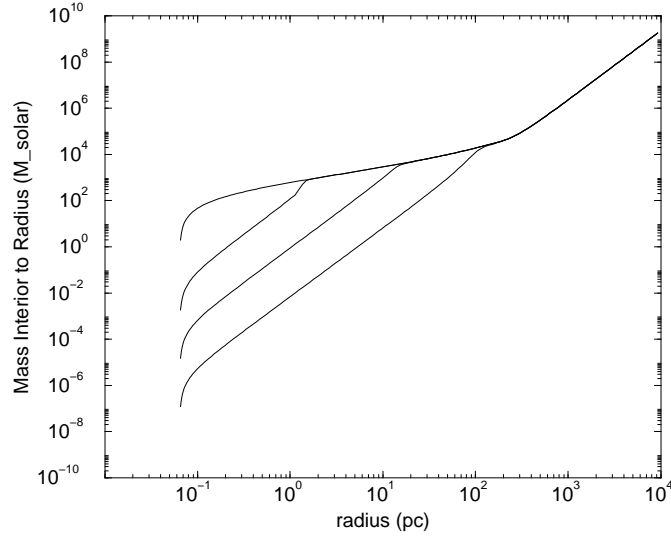


FIG. 5.— Mass interior to a given radius for $t = 63$ kyr, 317 kyr, and 2.2 Myr. The uppermost line is for the initial undisturbed density.

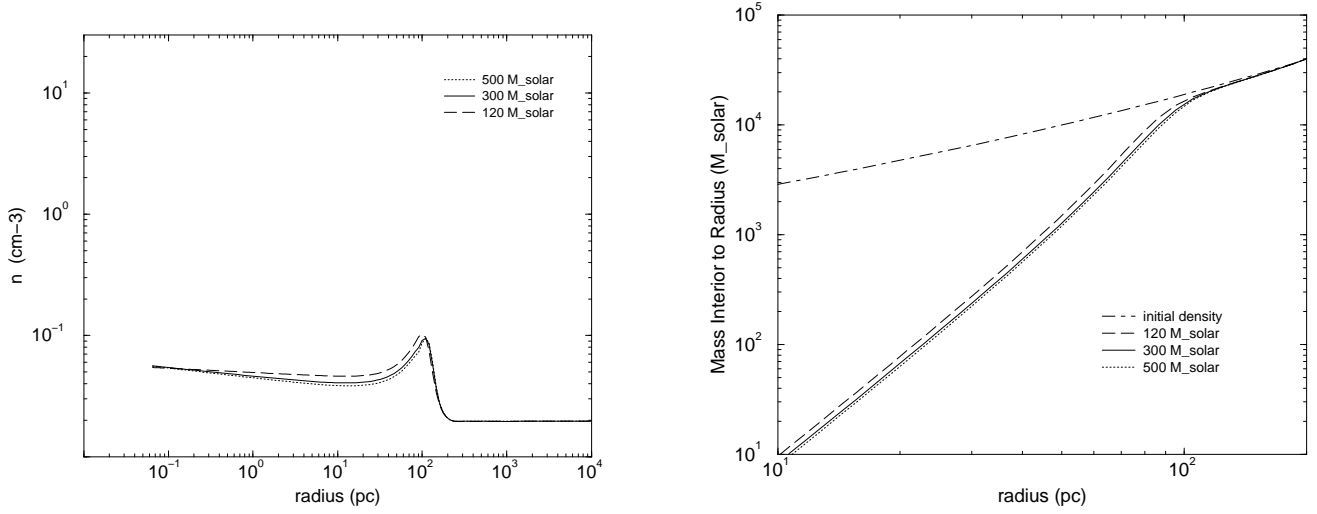


FIG. 6.— Left panel: Density distributions of $120 M_{\odot}$, $300 M_{\odot}$, and $500 M_{\odot}$ star HII regions permitted to flow out to 2.5 Myr. Right panel: Gas mass interior to a given radius again, but at the 2.5 Myr main sequence lifetime of a $120 M_{\odot}$ star.

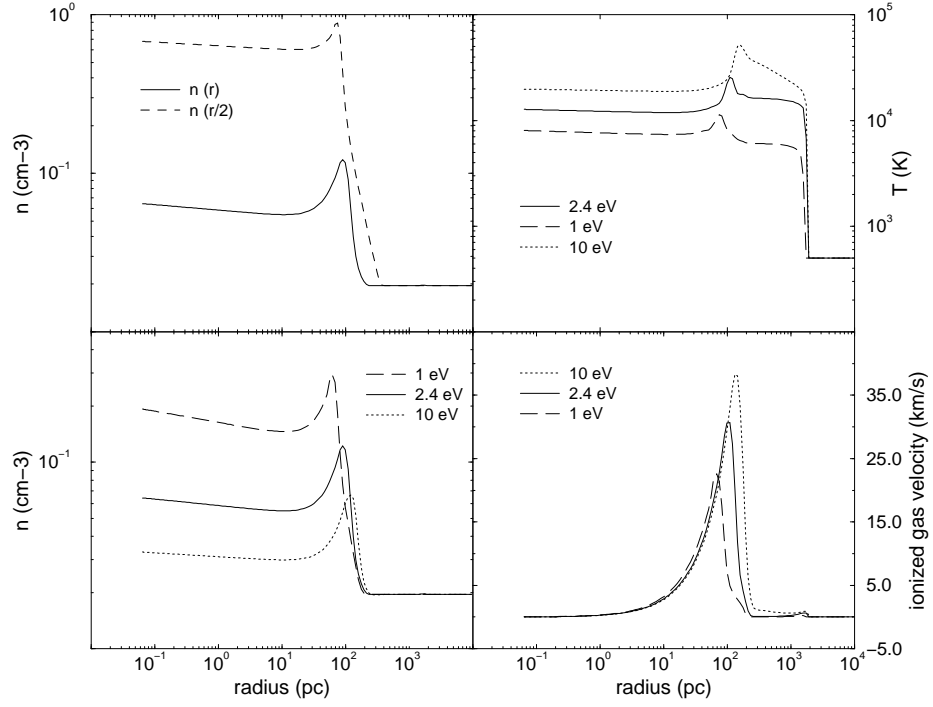


FIG. 7.— Upper left panel: HII region density profiles for a $200 M_{\odot}$ central star residing in the original Abel *et al.* (2002) halo density profile $n(r)$ and within a more massive halo $n(r/2)$. The densities shown are for 2.2 Myr. Upper right panel: temperature profiles for 1 eV, 2.4 eV, and 10 eV energy depositions into the gas, taken at 2.2 Myr. Lower panels: density (left) and velocity (right) plots for 1 eV, 2.4 eV, and 10 eV at 2.2 Myr.

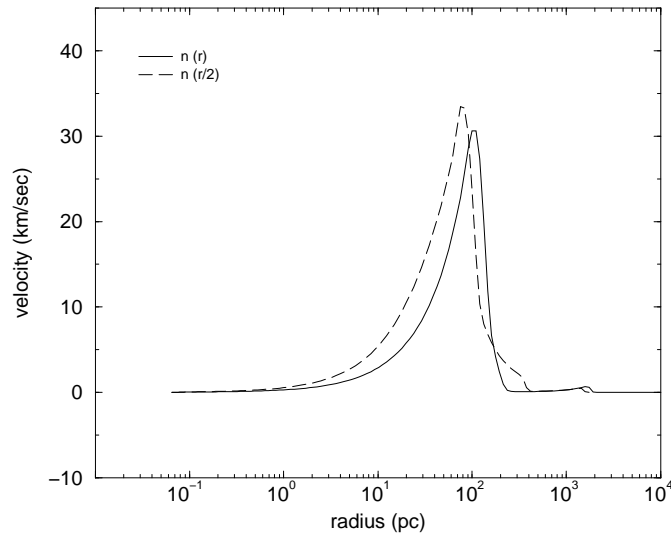


FIG. 8.— Ionized core shocks in the original Abel *et al.* (2002) halo density profile $n(r)$ and in a more massive halo $n(r/2)$

5.3. He Ionization

Our use of monochromatic radiative transfer underestimates the UV photoheating of the halo envelope by not accounting for the greater average energies imparted to electrons by the photons well above threshold emitted by the Pop III VMS. If only hydrogen were present this would be a relatively minor effect because of the ν^{-3} falloff of the ionization cross section. Neglecting primordial He ionization is more serious because it is heated to much higher temperatures than hydrogen by the harder photons in the stellar spectrum, though there are less of these photons as seen in Table 3.

Abel & Haehnelt (1999) have shown that one can approximate the heat input of He ionization by increasing the fixed amount of heat ϵ_{Γ} deposited by the radiation per photoionization. They found the amount by which this heat should be increased is sensitive to the radiation environment but in general is between $0.5 E_{\text{ioniz}}$ and E_{ioniz} . Our calculations to this point all applied 2.4 eV of heat per ionization to the gas. Temperature, density, and velocity profiles for a 200 M_{\odot} star for energy depositions of 1 eV, 2.4 eV, and 10 eV per ionization are shown in Fig 7. Helium ionization raises the temperature to between 20,000 K and 50,000 K in the front and to 20,000 K behind the front. The accompanying increase in sound speed results in the higher shock speeds and lower densities seen in the 10 eV case, demonstrating that the main contribution of He ionization is to accelerate the photoevaporative flow of gas from the halo. Our results for 2.4 eV therefore represent a lower limit to this flow.

Table 3: H, He, and He⁺ Ionizing Luminosities (Schaerer 2002)

M_{\odot}	Q(H)	Q(He)	Q(He ⁺)
500	6.802e50	3.858e50	5.793e49
400	5.247e50	3.260e50	5.567e49
300	3.754e50	2.372e50	4.190e49
200	2.624e50	1.628e50	1.487e49
120	1.391e50	7.772e50	5.009e48

5.4. Halo Mass

An interesting question is whether a sufficiently massive halo is capable of trapping the HII region. The escape velocity has no direct effect on escape fraction because the fraction depends only on the reversion of the front back to R-type, not on whether any gas exits the halo. This transition will occur in any halo whose baryonic density drops off more steeply than $r^{-1.5}$, whether or not there is outflow from the halo (the Abel, et al densities as well as more recent Λ CDM profiles all decrease approximately as $r^{-2.5}$).

However, core densities could be sufficiently high in massive halos to prevent this transition from occurring before the main sequence lifetime of the central source, in which case the front would be trapped as an ultracompact (UC) HII region (Kurtz 2000). We tested three halo mass profiles with a 200 M_{\odot} star by scaling the original density profile of Abel *et al.* (2002) by factors of 2 and 5 ($n(r/2)$ and $n(r/5)$). The most massive halo confined the I-front to a 0.1 pc UC HII region while the $n(r/2)$ halo permitted the front to escape, as seen clearly in Figs 7 and 8. The front has slightly higher temperatures in the greater $n(r/2)$ density and thus develops higher shock speeds. However,

the delay in the D- to R-type transition keeps the core shock from reaching the same radius as in the original distribution.

The high central densities of the most massive halo prevent the reversion of the I-front from D-type to R-type before the star exits the main sequence. Only in this unrealistically limiting case does no UV (or therefore gas) escape the halo. Breakout occurs in the other two cases although it occurs later in the more massive of the two halos so less mass is ejected from it. The final I-sphere radius of the $n(r/2)$ halo is also smaller than the $n(r)$ I-sphere because the $n(r/2)$ halo exhibits its high f_{esc} for less time. Until the relationship between the mass of a minihalo and the central star that may accrete within it is better understood it will not be possible to make a precise determination of how many Pop III I-fronts achieve breakout, only that the majority of them do for a reasonable scaling of halo densities with stellar mass.

6. CONCLUSIONS

Realistic escape fractions from the first luminous objects are close to unity because the halos become nearly transparent to UV photons when ionized by the R-type front. This result is of particular importance because recent determinations of the electron-scattering optical depth of the cosmic microwave background radiation since recombination suggest an early period of reionization (Kogut et al. 2003). The very massive stars ($30 M_{\odot} \lesssim M_{\text{FS}} \lesssim 300 M_{\odot}$) emerging in recent numerical simulations in concert with large UV escape fractions may likely be large contributors to early reionization. The photoevaporative flows of the first stars will leave dark halos with low gas content regardless of whether these stars die in bright supernovae or form black holes (e.g. Heger & Woosley (2002), for an extended discussion). Since the typical expansion velocities of the flows we find are much larger than the halo escape velocity one cannot expect the gas to return within timescales in which the halo would merge again into larger objects. Black hole remnants of the first stars that created the HII region could not accrete significant mass in the low density environment their progenitors have created. This fact may be an important constraint for theories of supermassive black hole formation relying on constant feeding of stellar black hole remnants (e.g. Haiman & Loeb (2001) and references therein).

The HII region that evacuates the halo will also enhance metal enrichment of the halo and interhalo medium by the first supernova. A 200 M_{\odot} pair-instability supernova remnant initially expands into an ambient density that is only twice the interhalo mean. Fig 5 shows this ejecta must travel 10 pc before encountering its own mass in halo material, before which it would be in a free-expansion state. The remnant will not enter a Sedov-Taylor phase until it is at least 50 pc in radius, at which point Rayleigh-Taylor instabilities that we cannot simulate in 1D begin to mix the ejected metals with the gas in the halo. How these instabilities promote metal pollution of the early IGM will be the focus of future study. Only three dimensional models of the first HII regions will allow us to address the detailed questions recently raised by Oh & Haiman (2003).

We would like to thank the anonymous referee for suggestions that significantly improved the quality of this manuscript. This work was partially supported by NSF grants AST-9803137 and AST-0307690 to MLN. The calculations were carried out on NCSA's Origin2000 with NPAC allocation PQQ.

REFERENCES

- Abel, T. 1995, Thesis, University of Regensburg.
- Abel, T., Anninos, P., Zhang, Y., & Norman, M. L. 1997, *New Astronomy*, 2, 181
- Abel, T., Anninos, P., Norman, M. L., & Zhang, Y. 1998, *ApJ*, 508, 518
- Abel, T., Bryan, G. L., & Norman, M. L. 2002, *Science*, 295, 93
- Abel, T., Bryan, G. L., & Norman, M. L. 2000, *ApJ*, 540, 39
- Abel, T. & Haehnelt, M. G. 1999, *ApJ*, 520, L13
- Abel, T., Norman, M. L., & Madau, P. 1999, *ApJ*, 523, 66
- Anninos, P., Zhang, Y., Abel, T., & Norman, M. L. 1997, *New Astronomy*, 2, 209
- Baraffe, I., Heger, A., & Woosley, S. E. 2001, *ApJ*, 550, 890
- Barkana, R. & Loeb, A. 2003, *ApJ*, submitted (astro-ph/0305470)
- Bromm, V., Coppi, P. S., & Larson, R. B. 1999, *ApJ*, 527, L5
- Burles, S. & Tytler, D. 1998, *ApJ*, 499, 699
- Cen, R. 2003, *ApJ*, 591, 12
- Ciardi, B., Ferrara, A., Marri, S., & Raimondo, G. 2001, *MNRAS*, 324, 381
- Ciardi, B., Ferrara, A., & White, S. D. M. 2003, *MNRAS*, 344, L7
- Dove, J. B., Shull, J. M., & Ferrara, A. 2000, *ApJ*, 531, 846
- Franco, J., Tenorio-Tagle, G., & Bodenheimer, P. 1990, *ApJ*, 349, 126
- Fujita, A., Martin, C. L., Mac Low, M., & Abel, T. 2003, *ApJ*, 599, 50
- Fuller, T. M. & Couchman, H. M. P. 2000, *ApJ*, 544, 6
- Haiman, Z. & Holder, G. P. 2003, *ApJ*, 595, 1
- Haiman, Z. & Loeb, A. 2001, *ApJ*, 552, 459
- Heger, A. & Woosley, S. E. 2002, *ApJ*, 567, 532
- Hurwitz, M., Jelinsky, P., & Dixon, W. V. D. 1997, *ApJ*, 481, L31
- Kogut, A. et al. 2003, *ApJS*, 148, 161
- Kudritzki, R. 2000, The First Stars. Proceedings of the MPA/ESO Workshop held at Garching, Germany, 4-6 August 1999. Achim Weiss, Tom G. Abel, Vanessa Hill (eds.), Springer, p.127, 127
- Kurtz, S. E. 2000, *Revista Mexicana de Astronomia y Astrofisica Conference Series*, 9, 169
- Leitherer, C., Ferguson, H. C., Heckman, T. M., & Lowenthal, J. D. 1995, *ApJ*, 454, L19
- Machacek, M. E., Bryan, G. L., & Abel, T. 2001, *ApJ*, 548, 509
- Oh, S. P. & Haiman, Z. 2003, *MNRAS*, 346, 456
- Omukai, K. & Inutsuka, S. 2002, *MNRAS*, 332, 59
- Omukai, K. & Palla, F. 2003, *ApJ*, 589, 677
- Osterbrock, D. *Astrophysics of Gaseous Nebulae and Active Galactic Nuclei*, University Science Books 1989.
- Palla, F., Salpeter, E. E., & Stahler, S. W. 1983, *ApJ*, 271, 632
- Ricotti, M. & Shull, J. M. 2000, *ApJ*, 542, 548
- Schaerer, D. 2002, *A&A*, 382, 28
- Silk, J. 1983, *MNRAS*, 205, 705
- Sokasian, A., Abel, T., Hernquist, L., & Springel, V. 2003, *MNRAS*, 344, 607
- Somerville, R. S. & Livio, M. 2003, *ApJ*, 593, 611
- Spergel, D. N. et al. 2003, *ApJS*, 148, 175
- Steidel, C. C., Pettini, M., & Adelberger, K. L. 2001, *ApJ*, 546, 665
- Tenorio-Tagle, G., Bodenheimer, P., Lin, D. N. C., & Noriega-Crespo, A. 1986, *MNRAS*, 221, 635
- Vink, J. S., de Koter, A., & Lamers, H. J. G. L. M. 2001, *A&A*, 369, 574
- Wise, J. H. & Abel, T. 2002, *American Astronomical Society Meeting*, 201
- Wood, K. & Loeb, A. 2000, *ApJ*, 545, 86
- Yoshida, N., Abel, T., Hernquist, L., & Sugiyama, N. 2003, *ApJ*, 592, 645